RSC Advances

PAPER

View Article Online
View Journal | View Issue

Cite this: *RSC Adv.*, 2016, **6**, 53873

Low-voltage electro-optical memory device based on NiO nanorods dispersed in a ferroelectric liquid crystal†

Achu Chandran,*[ab] Jai Prakash,[c] Jitendra Gangwar,[bd] Tilak Joshi,[b] Avanish Kumar Srivastava,[b] D. Haranath[ab] and Ashok M. Biradar[ab]

Received 14th February 2016
Accepted 25th May 2016

DOI: 10.1039/c6ra04037c

www.rsc.org/advances

We present a low voltage driven electro-optical memory device fabricated by dispersing nano-sized nickel oxide (nNiO) composed of short length nanorods into a ferroelectric liquid crystal (FLC) host material. The nNiO/FLC composite showed a tremendous decrease in saturation voltage compared to the pristine FLC material along with non-volatile memory behavior which is confirmed through dielectric spectroscopy, polarized optical microscopy and electro-optical response methods. This drop off in saturation voltage is due to the fast alignment of dipolar nNiO and mesogens in the nNiO/FLC composite along the direction of the applied electric field and reduced screening effect. The non-volatile memory behavior of the composite is attributed to the reduction in the depolarization field by adsorption of impurity ions onto the surface of nNiO, which is verified through dielectric spectroscopy and electrical conductivity measurements. These studies pave the way for fabricating non-volatile, low power electro-optical memory devices for advanced information storage applications.

Introduction

The memory effect shown by soft materials has attracted wide research attention due to its fundamental and applied aspects.[1–3] The term memory in soft materials refers to the ability of the material to retain the stressed/switched state even after the removal of an external stimulus. Various forms of memory exhibited by soft materials include digital memory shown by bio-nano composites,[1] multilevel non-volatile transistor memory,[4] the re-writable shape memory effect of polymeric materials,[5] soft memory based on magneto-electric coupling in polymer forms[6] *etc.* Recently, non-volatile, low power memory devices are being fabricated by using regular arrays of a highly ordered nano-structured ferroelectric polymer.[7] Among the members of the soft matter family, liquid crystals (LCs) have attracted a great deal of scientific interest owing to their unique electro-optical properties for displays as well as non-display applications such as lenses, spatial light modulators, antennas, sensors *etc.*[8–11] Also, the soft memory behavior shown by LCs are fascinating one due to its use as an active component for futuristic and motivating memory devices. The non-volatile memory seen in different LC systems are the topological frustrations driven memory effect in nematic LC,[12,13] sub microsecond bistable electro-optic switching in surface stabilized ferroelectric liquid crystal (FLC),[14] electro-mechanical helix deformations in deformed helix FLCs,[15] nano structured materials induced electro-optical memory effect in LCs[16] *etc.* Although this memory effect in LCs was reported many years ago, its exact physical behavior is not explained yet. FLCs, the highly potential member of LC family is well-known for their good optical contrast, fast response time, low operational voltage and memory effect.[17] But, the memory behavior of most of the FLCs is found to be transient in nature.

Dispersion of NPs in LCs is mutually beneficial as the properties of both can be tailored by adequate doping concentration.[18] A variety of nano structured materials including metal nanoparticles (NPs),[19] metal oxide NPs,[20] ferroelectric NPs,[21] carbon nanotubes,[22] quantum dots[23] *etc.* have been used to improve the memory behavior of LCs. As a dopant to LCs, metal oxide NPs are well known for their unique physical and chemical properties owing to their limited size and high density of corners.[24] On dispersing SiO_2 NPs into nematic[25] and smectic[26] LCs induced a memory effect owing to the hydrogen bonds between the individual silica particles. Recently, it is seen that ZrO_2 NPs/FLC composites showed a non-volatile memory behavior due to adsorption of impurity ions on to the surface of NPs.[20] Apart from imparting the memory effect, dispersing the nano structures into the LCs have improved the molecular alignment, dielectric and

[a]*Academy of Scientific and Innovative Research (AcSIR), CSIR-National Physical Laboratory Campus, Dr. K. S. Krishnan Road, New Delhi-110012, India. E-mail: ac60369@gmail.com; chandraa@nplindia.org*

[b]*CSIR-National Physical Laboratory, Dr. K. S. Krishnan Road, New Delhi-110012, India*

[c]*Department of Physics, Aligarh Muslim University, Aligarh-202002, Uttar Pradesh, India*

[d]*Department of Physics, The IIS University, Jaipur-302020, India*

† Electronic supplementary information (ESI) available. See DOI: 10.1039/c6ra04037c

electro-optical characteristics of the host material such as enhanced optical contrast, faster response time, low operational voltage *etc*.[16] Also, low power operating devices are highly appreciable since the saving of energy is equally important as that of production. Metal oxide NPs such as TiO_2 and ZnO when dispersed in nematic and smectic LCs respectively has shown their potential for low power LC device operation.[27,28]

Among the metal oxide nanostructures, nano-sized NiO (nNiO) has been used as a promising candidate in wide range of technological applications including catalytic convertors, nano magnetic and spintronic devices for memory and computing, sensors, supercapacitors *etc*.[29–32] This versatile material has exciting properties such as transparent conduction, magnetism and resistance switching which renders its use in spintronics and resistive random access memories.[33–35] Recent efforts are made to evaluate the performance of nNiO in nematic LC, in which it is seen that twisted nematic LC doped with nNiO exhibited lower threshold voltage and faster response time.[36] To the best of our knowledge, this is the first attempt to elucidate the effect of nNiO dispersions on the bistability and electro-optical properties of FLC.

Here in, we propose a device based on nNiO/FLC composite which ends the quest for low voltage driven memory device based on LCs. The low power operating non-volatile memory behavior of the composite is confirmed through dielectric spectroscopy, polarized optical microscopy and electro-optical response methods. The enhanced bistability of the composite is due to the reduced depolarization field by adsorption of ions in the host FLC and the reduction in saturation voltage is owing to the fast aligning of dipolar nNiO and mesogens in the composite along the applied electric field and reduced screening effect of ionic impurities. The nNiO/FLC composite can be utilized for fabricating advanced e-book readers and notice boards which are low voltage triggered electro-optic memory devices.

Experimental

Synthesis of nNiO

The nNiO composed of short length nanorods are fabricated from a wet chemical solution method. Nickel nitrate hexahydrate ($Ni(NO_3)_2 \cdot 6H_2O$; 98%, Merck, AR) and ammonia solution (NH_4OH; 25%, Rankem) are the main precursors used for the synthesis of nNiO. A typical synthesis of nNiO was carried out as follows. A green aqueous solution of $Ni(NO_3)_2 \cdot 6H_2O$ (0.5 M) was first prepared. The pH of this solution was adjusted at the value of 10 by adding NH_4OH (2 M) solution dropwise under constant stirring maintaining a constant temperature of 85 °C. The light green coloured precipitate was filtered off and washed repeatedly by millipore water and ethanol followed by micro-oven drying at 70 °C for 24 h. To obtain the nNiO, the resultant light green powder was calcined at 400 °C for 2 h inside a muffle furnace.

Details of FLC material used

The FLC material used in this study is ZLI 3654, which is a room temperature FLC mixture procured from E. Merk, Darmstadt.[37] The phase sequence of the FLC material, ZLI 3654 is as follows:

$$\text{cryt} \xleftrightarrow{<-30\ ^\circ\text{C}} \text{SmC*} \xleftrightarrow{62\ ^\circ\text{C}} \text{SmA*} \xleftrightarrow{76\ ^\circ\text{C}} \text{N*} \xleftrightarrow{86\ ^\circ\text{C}} \text{iso}$$

where, cryst is the crystalline phase, SmC* is chiral smectic C phase, SmA* is the chiral smectic A phase, N* is the chiral nematic phase, and iso is the isotropic phase.

Preparation of nNiO/FLC composite

The LC sample cells used to fill the composite have been fabricated by using highly conducting (30 ohms per square) and optically transparent sputtered indium tin oxide (ITO) glass substrates. The desired (square) electrode patterns having the area 0.45 cm × 0.45 cm were obtained by using photolithographic (using positive photoresist) technique. The homogeneous alignment of LC sample cells has been achieved by using conventional rubbed polyimide technique. The thickness of the cell was maintained by using 7 μm thick Mylar spacers.

The nNiO/FLC composite was prepared by dispersing various concentrations (wt%) of nNiO into the FLC host material, ZLI 3654. The mixture was then ultrasonicated for about 40 min in the isotropic phase of the FLC material to ensure the homogeneous dispersion of nNiO in the FLC host. The pristine and nNiO (of different concentration) dispersed ZLI 3654 material were then introduced into the LC sample cells by means of capillary action at temperature just above the isotropic transition temperature of ZLI 3654.

Apparatus and measurements

The dielectric spectroscopic measurement for confirming the memory effect in sample cells has been done by using impedance analyzer (Wayne Kerr 6540 A, U. K) in a frequency window of 20 Hz to 1 MHz with a measuring voltage of 0.5 V_{pp}. A temperature controller (JULABO F-25 HE) was used for controlling the temperature with a temperature stability of ±0.01 °C. The sample holder containing the sample cells was kept thermally isolated from the external sources for carrying out the temperature dependent studies. The optical tilt angle and micrographs of the sample cells were taken with the help of polarized optical microscope (POM) (Ax-40, Carl Zeiss, Germany) fitted with charge coupled device (CCD) camera. The material parameters of FLC sample cells such as rotational viscosity and spontaneous polarization are determined by using an automatic liquid crystal tester (ALCT, Instec, USA). For optical response, the sample was mounted on a polarizing microscope and the transmission of normally incident polarized light through the sample and analyzer was monitored with a photodiode. The time delayed square pulse generated from the function generator was applied to the sample and studied by using a storage oscilloscope (HAMEG, HM 1507-3) interfaced with the computer *via* SP-107 software. Powder X-ray diffraction (XRD) pattern was collected on a Rigaku Miniflex-II X-ray diffractometer using the Cu-Kα monochromatic radiation (λ = 1.541 Å), in the 2θ range between 10.07 and 70.07°. The structural refinement for refining the crystalline structure of NiO was determined by the Rietveld method using the program FULLPROF. The morphological identification and size were examined using a high-resolution transmission electron microscopy

analysis and selected-area electron diffraction (SAED) pattern were acquired with a high resolution transmission electron microscope (HRTEM) (FEI Tecnai G2 F30 STWIN) operated at the electron accelerating voltage of 300 kV using electron source as field emission gun.

Results and discussions

We demonstrate the crystallographic structural characteristics and electron microscopy of the NiO nanorods in Fig. 1(a)–(c). The XRD pattern of NiO nanorods (Fig. 1(a)) is compared with Joint Committee on Powder Diffraction Standards (JCPDS) file and found matching with JCPDS no. 71-1179. Thus the product has cubic NiO of space group $Fm\bar{3}m$ with lattice parameters $a = b = c = 0.4178$ nm (standard JCPDS no. 71-1179). Moreover, the identified peak positions and relative intensity of peaks observed in XRD pattern were sharp and intense indicating good crystallinity and high purity of NiO nanorods. Also, the experimental XRD pattern of nNiO is simulated by Rietveld refinement and the details of which is given as ESI.† The ball-and-stick representative unit cell with the observed planes in XRD pattern of nNiO illustrated in Fig. 1(a) (inset in Fig. 1(a)) has a cubic crystal structure in octahedral environment of the Ni^{2+} ($3s^2 3p^6 3d^8$) imposed by the six neighboring oxygen (O^{2-}) atoms. The morphology and size of nanorods has been evaluated by HRTEM analysis. Fig. 1(b) shows the bright-field TEM micrograph of NiO nanorods. The result obtained using TEM elucidated the presence of uniform short-length nanorods of length between 12 and 30 nm with 6 nm in width. The HRTEM image (Fig. 1(c)) elucidates the stacking of (200) planes with the interplanar spacing of about 0.22 nm of NiO nanorods reveals the good consistency with the observed XRD pattern. The inset in Fig. 1(c) displays the SAED pattern of NiO nanorods establishes the polycrystalline nature of the sample.

Fig. 2 shows the POM images (dark and bright state) of homogeneously aligned LC cells filled with pure and various concentrations (0.25 wt%, 0.5 wt% and 1 wt%) of nNiO dispersed FLC material ZLI 3654 at room temperature (27 °C).

The dark and bright state of pristine FLC material (Fig. 2(a) and (b)) exhibit a non-uniform alignment of mesogens owing to

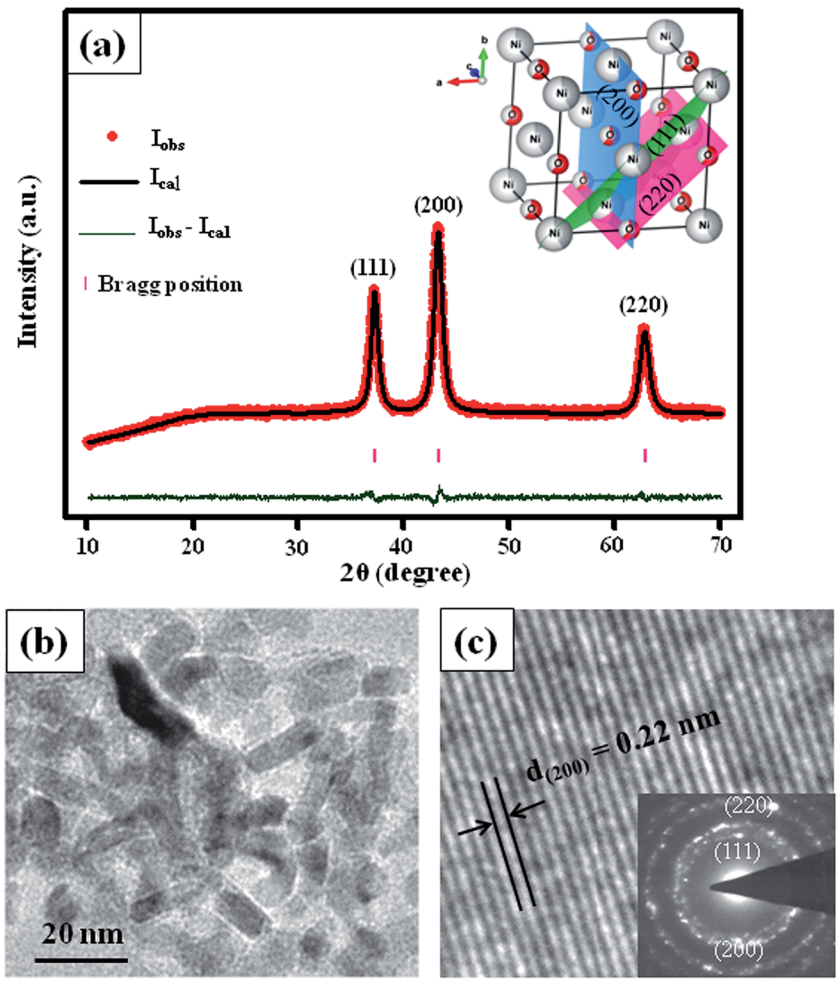

Fig. 1 (a) Rietveld-refined XRD pattern of NiO nanorods, (b) bright-field TEM image at low magnification, (c) high-resolution TEM micrograph showing the lattice fringe scaling of the sample. Insets: (a) the cubic crystal structure of NiO with the observed planes from XRD pattern, (c) the corresponding SAED pattern. Color code: (inset in a) Ni atoms, gray (large balls) and O atoms, red (small balls); planes (111), (200) and (220) are drawn in green, blue and pink rectangles, respectively.

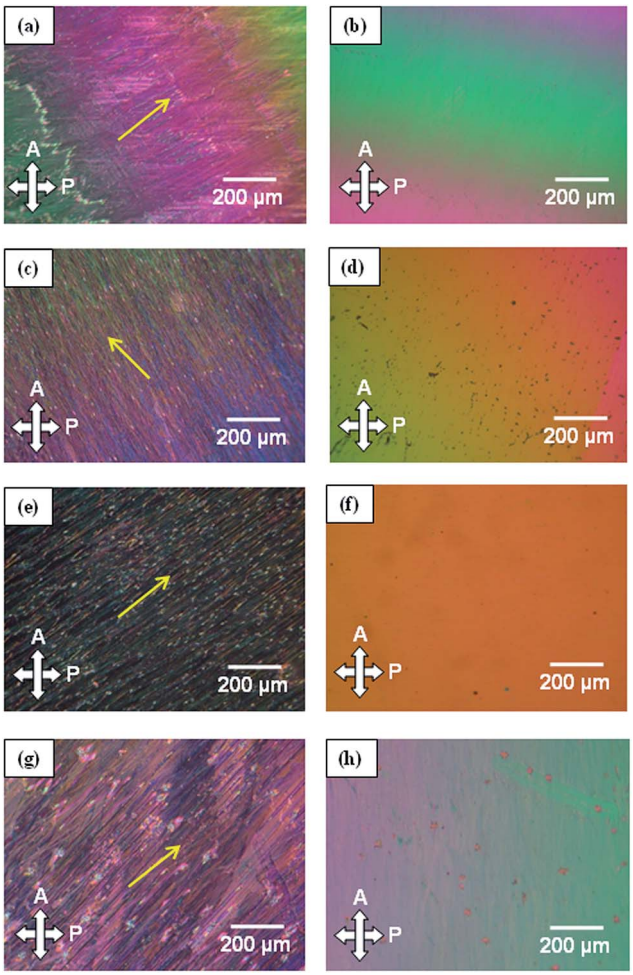

Fig. 2 Polarizing optical micrographs of (a) dark, (b) bright state of pure ZLI 3654 material; (c) dark, (d) bright state of 0.25 wt% nNiO dispersed ZLI 3654 material; (e) dark, (f) bright state of 0.5 wt% nNiO dispersed ZLI 3654 material; and (g) dark, (h) bright state of 1 wt% nNiO dispersed ZLI 3654 material filled LC sample cells of 7 μm thickness under crossed polarisers at room temperature (27 °C) (rubbing direction of each sample cell is indicated as yellow arrow).

the zig–zag defects present in the cell. The sharp edges of these defects allow the light transmission in the dark state of the LC cell, which is seen in Fig. 1(a), and degrades the performance of display devices. But on dispersing various concentrations of nNiO on to the host FLC material, ZLI 3654, the defect got reduced and a better alignment of mesogens is observed. Among the nano-dispersed samples, 0.5 wt% nNiO dispersed FLC cell showed the best dark and bright states as demonstrated in Fig. 2(e) and (f). The shape anisotropy of nNiO and its dipolar nature is responsible for the improved alignment of mesogens. When the concentration of nNiO was higher (1 wt%), the alignment of LC molecules got distorted due to the agglomeration of nNiO resulting in light leakage in dark state (Fig. 2(g)) and dark spot type appearances in bright state (Fig. 2(h)). So, the optimum dispersion concentration of nNiO is 0.5 wt% for electro-optical display based applications, where good molecular alignment of FLC is seen.

Further the pristine and nNiO/FLC composite samples were characterized for their material parameters. Fig. 3 illustrates the changes in material parameters of pristine FLC material such as optical tilt angle (θ), spontaneous polarization (P_s), rotational viscosity (γ) and response time (τ) with applied voltage due to dispersing nNiO into it.

For FLCs, θ is the primary order parameter, which increases with increasing the applied voltage owing to the coupling of P_s with applied electric field and attains a saturation value at a particular applied voltage called saturation voltage (V_{sat}). From Fig. 3(a), it is evident that saturation value of θ is ~22° for both pure and composite samples. Interestingly, the V_{sat} value for pure FLC sample is ~8 V, whereas the θ of nNiO/FLC composite got saturated at an applied voltage of ~4 V. *i.e.*, at half the voltage of pristine FLC cell. Thus, nNiO/FLC composite device can be operated in half the voltage of the pristine FLC, which saves almost ~50% of operating power. As evident from Fig. 3(b)–(d), the saturation value of P_s, γ and τ is ~29 nC cm^{-2}, ~380 mPa s and ~1 ms respectively for the pure FLC material, ZLI 3654. On dispersing nNiO into ZLI 3654, the composite showed a reduction in saturation value of P_s and γ. The value of τ is decreased for nNiO dispersed FLC sample, since P_s, γ and τ are related to each other as shown in eqn (1).

$$\tau = \gamma/(P_s E) \quad (1)$$

where, τ is response time, γ is the rotational viscosity, P_s is the spontaneous polarization, and E is the applied electric field respectively.

Dielectric spectroscopy is a promising tool for confirming the memory behavior in an LC sample cell. Fig. 4 shows the dielectric dispersion spectra at room temperature of pristine and nNiO/FLC composite sample at room temperature (27 °C).

In Fig. 4(a), it is seen that in pure FLC sample cell, when an external DC bias of 15 V is applied, the dielectric permittivity (ε') decreases to a minimum value due to suppression of phason mode, which occurs due to the phase fluctuation of the mesogens. On removal of external DC bias, ε' gets back to its initial value within 1 minute. Thus, the memory behaviour of pure FLC material ZLI 3654 is transient in nature. But, on comparing with nNiO/FLC composite, it is seen that (Fig. 4(b)), the composite stayed in memory state for up to 10 minutes. Also, the transit from stressed state to relaxed state was gradual. This indicates almost tenfold increment in memory behaviour of pure FLC material by dispersing nNiO into it.

In order to confirm and observe the duration of the electro-optic memory state in nNiO/FLC composite, POM images of the composite is taken by applying and then removing the DC bias. Fig. 5 shows POM images of nNiO/FLC composite in dark and switched (bright) states at room temperature.

The composite cell is initially set to dark state (Fig. 5(a)) under POM without any external bias. It is then switched to bright state by application of 15 V DC bias as shown in Fig. 5(b). As the bias field is switched off, the nNiO/FLC composite cell was able to retain the bright state up to ~20 min as evident from Fig. 5(c)–(f). Thus, the observed memory state is recorded after removal of bias under POM at different time intervals of 10 s, 2

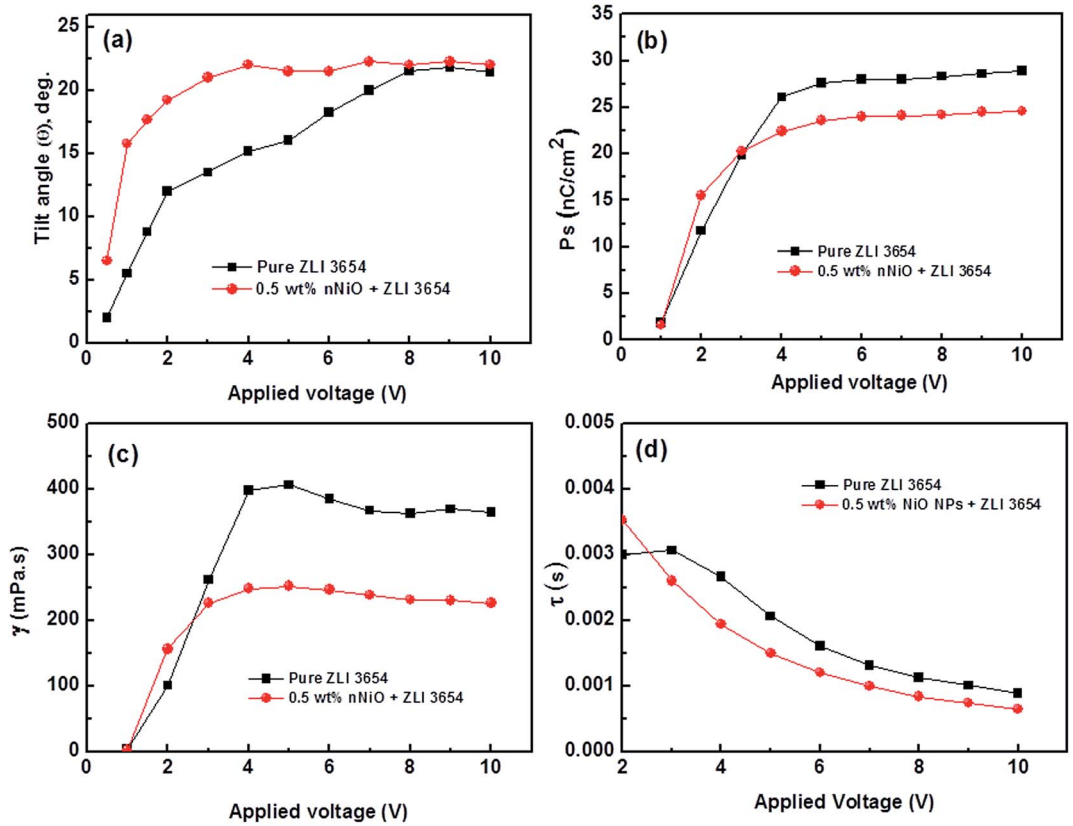

Fig. 3 Behaviour of (a) tilt angle (θ), (b) spontaneous polarization (P_s), (c) rotational viscosity (γ), and (d) response time (τ) of pure FLC material, ZLI 3654 and nNiO/FLC composite material filled sample cells of 7 μm thickness at room temperature (27 °C).

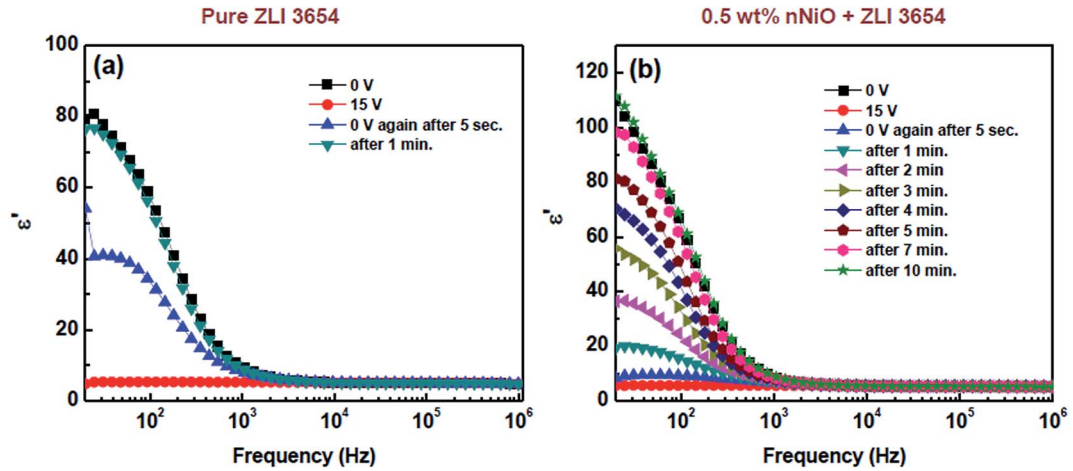

Fig. 4 Dielectric dispersion spectra (dielectric permittivity, ε', as a function of frequency) of (a) pure FLC material, ZLI 3654 and (b) nNiO/FLC composite filled sample cell of 7 μm thickness showing the duration of dielectric memory state at room temperature (27 °C).

min, 10 min and 20 min respectively (Fig. 5(c)–(f)). The surface anchoring forces imparted by the alignment layer along with the elastic forces of mesogens are responsible for bringing the FLC molecules back to the initial dark state.

The electro-optical memory effect seen in nNiO/FLC composite is further verified by optical response. Fig. 6 demonstrates the optical response of pristine and nNiO dispersed FLC sample cell by applying a time delayed positive and negative square pulse of 20 V_{pp} at 100 Hz.

In the optical response of pure FLC sample cell, the output waveform was simply following the input signal, which shows the transient memory behavior in pristine FLC material [Fig. 6(a)]. But, in nNiO/FLC composite sample cell (Fig. 6(b)), the optical transmission remains in the maximum state even

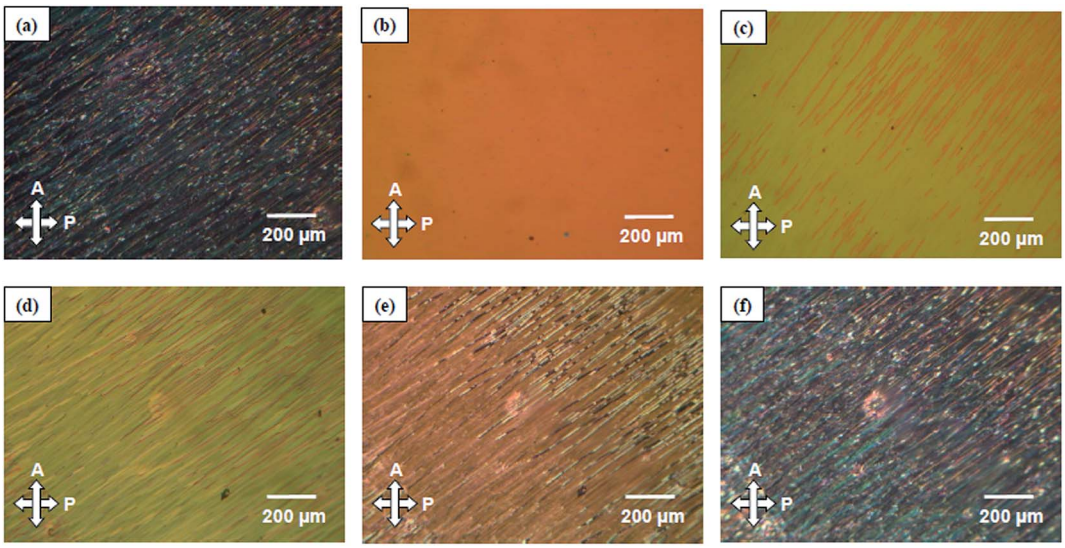

Fig. 5 Polarizing optical micrographs showing the duration of electro-optical memory state of nNiO/FLC composite material filled sample cell. The images of composite sample cell at (a) 0 V DC bias, (b) 15 V DC bias, (c) 10 seconds after removal of bias, (d) 1 minute after removal of bias (e) 10 minutes after removal of bias and (f) 20 minutes after removal of bias at room temperature (27 °C).

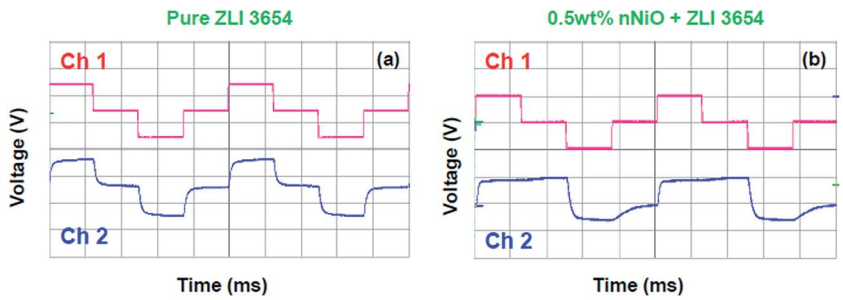

Fig. 6 Optical response of (a) pure FLC material, ZLI 3654 and (b) nNiO/FLC composite material filled sample cells to a driving time delayed positive and negative square pulse of 20 V_{pp} at 100 Hz. Ch1 (Ch1: 10 V per div, Ch2: 5 V per div, time: 5 ms) shows the input square pulse and Ch2 shows its optical response. The time scale per division is shown on *x*-axis, which is same for both channels.

the input waveform switched to zero state (0 V). This behavior is repeated for the negative pulse also. Thus, optical response method gave yet another confirmation of the electro-optical memory behavior of nNiO/FLC composite sample cell.

It is interesting to elucidate the underlying mechanism of enhancement in electro-optical memory of FLC material, ZLI 3654 by dispersing nNiO. Previous reports on bistability of FLC device reveals that, it is greatly influenced by the impurity ions containing in it.[38] In spite of its mobility, impurity ions are always detrimental to the bistability of FLCs. The ionic impurities accumulated in between the alignment layer and FLC medium enhances the depolarization field and accelerate the decay of bistability when the electric field is switched off. Also, the overall performance of FLC devices based on ZLI 3654 material is degraded by the selective ion adsorption by the alignment layers.[39] The gray-level shift, image sticking/flickering problem and slow response to electric field are also caused by ionic impurities present in LCs. In an LC device, sources of impurity ions are LC material itself, through atmosphere or alignment layer, during synthesis process *etc.* The anchoring energy of mesogens and driving voltage of LC devices get altered owing to the presence of impurity ions in it.[39,40]

It is worth to study the electrical conductivity and dielectric absorption spectrum of the pristine and nNiO/FLC composite sample cells to get inference about the ionic impurity content in the sample cells. Fig. 7 presents the dielectric absorption and electric conductivity with frequency for pure and nNiO/FLC composite sample cells at room temperature (27 °C).

In dielectric absorption (tan δ) spectrum (Fig. 7(a)), it is seen that the pristine FLC material, ZLI 3654 shows two types of dielectric relaxation peaks at room temperature, goldstone mode (GM)[37] relaxation peak and a low frequency dielectric relaxation peak. The GM relaxation process occurs due to phase fluctuations of mesogens in the smectic C* phase of FLCs near to ~1 kHz and the low frequency dielectric relaxation peak centered at ~40 Hz is owing to the ionic impurities contained in the FLC materials. This ionic relaxation process in FLCs may occur due to ionization–recombination assisted diffusion of slow ions or single particle diffusion of fast ions.[41] But, on dispersing nNiO into ZLI 3654, it is seen that (Fig. 7(a)) the ionic

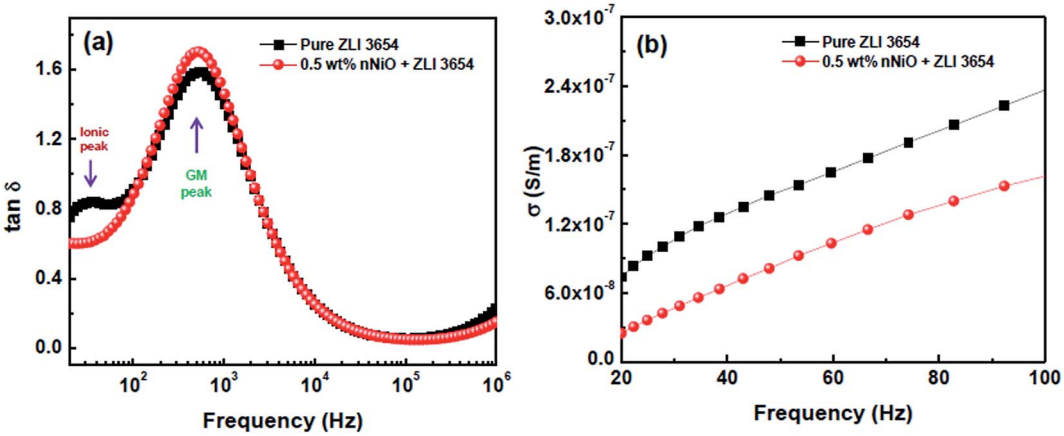

Fig. 7 (a) Dielectric absorption spectra (dielectric loss factor, tan δ, with frequency) and (b) behavior of electrical conductivity (σ) with frequency of pure FLC material, ZLI 3654 and nNiO/FLC composite material filled cell of 7 μm thickness at room temperature (27 °C).

impurity peak is disappeared and only GM peak is visible. This screening effect of ionic impurities in the composite sample cell is due to adsorption or trapping of the same by nNiO. Similar reports are there in which the effect of ionic impurities in LC materials are reduced by adsorption/trapping phenomenon using different types of nano-sized species including Al_2O_3, ZrO_2, TiO_2, ZnO, carbon nanotubes, diamond powders *etc.*[20,42–45] In nano-structured NiO, there are plenty of defects such as structural and compositional defects and the control over those defects will lead to tailor the properties of NPs.[46] It is well known that, the defect structures seen on the surface of metal oxide NPs are attributed to incomplete oxidation of hydroxide species during synthesis process. Here, during the synthesis process of nNiO from the precursors, $Ni(OH)_2$ is formed as an intermediate compound. This $Ni(OH)_2$ undergoes decomposition/dehydration during the calcination process to produce nanoparticulate cubic NiO. The dehydration process is accompanied by oxolation mechanism and subsequently forms O–Ni–O bridges.[47] Thus, improper calcination leads to unsaturated OH groups, anionic and cationic vacancies on the surface of nNiO. Also, nNiO has proven its ability to adsorb ionic impurities from aqueous solutions on to the active sites on its surface.[48,49] These active sites are composed of either nickel or oxygen vacancies.[50,51] Several mechanisms including surface complexation, cation exchange and electrostatic attraction are responsible for the strong adsorption affinity of nano sized NiO to ionic species.[48] Impurities with organic or polar functional groups are strongly adsorbed onto the surface of nano sized NiO containing hydroxyl moieties ($-OH_2^+$, –OH, $-O^-$) *via* charge–charge or electronic coupling interactions.[52] Here also, the unsaturated surface sites of nNiO are responsible for the trapping/adsorption of ionic impurities contained in FLC material ZLI 3654.

The adsorption/trapping of ions in the nNiO/FLC composite is again confirmed through the electrical conductivity (σ) studies of the pure and composite samples, as the σ in LCs is only due to ions contained in it. As illustrated in Fig. 7(b), the σ of nNiO/FLC composite is less than the pristine FLC material. On comparing the values, the σ of pure ZLI 3654 is $\sim 1.3 \times 10^{-7}$ S m^{-1} at 40 Hz and that of the composite sample cell is $\sim 0.66 \times 10^{-7}$ S m^{-1} *i.e.*, almost ~50% decrement in the σ. This drop off in σ is due to the adsorption/trapping of ionic impurities in the pure ZLI 3654 material by nNiO.

The mechanism behind low voltage driven enhanced electro-optical memory behavior by trapping of impurity ions is schematically illustrated in Fig. 8. The nNiO/FLC composite material is sandwiched in between the ITO coated glass plates with

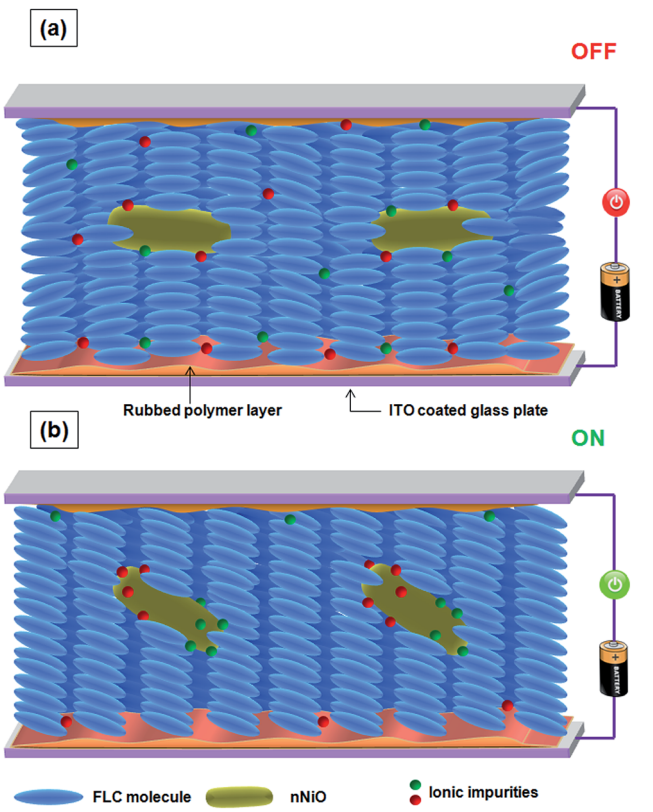

Fig. 8 Schematic depiction of mechanism of memory behavior in nNiO/FLC composite material filled sample cell. The homogenously aligned composite sample cell at (a) OFF and (b) ON state of external DC bias.

rubbed polymer (nylon 6/6) layer for homogeneous alignment of mesogens is seen in Fig. 8(a).

The ionic impurities which arise from FLC material, alignment layer and atmosphere are randomly distributed over the volume. It is reported that nNiO possess a permanent dipole moment along [111] plane.[53,54] The nNiO used in our study for preparing the composite is also having [111] plane (JCPDS no. 71-1179). Since the mesogens and nNiO are dipolar in nature, the FLC molecules get aligned along the nNiO owing to the effective dipole–dipole interaction which leads to the improved alignment of composite device. Also, nanorods possessing inherent dipole moment can align faster with mesogens due to large torque experienced in external bias field, which results in reduction in V_{sat}.[55] When electric field is switched on, the dipolar mesogens and nNiO get aligned along the direction of field as shown in Fig. 8(b). Mean while the mobile ionic impurities will travel to the opposite electrodes according to their charge. In the case of pristine FLC material ZLI 3654, these impurity ions will add to the depolarization field and enhances the screening of external bias field. Thus, more external voltage is required to switch on the pristine display device (~8 V). Also, when the display is switched off, the mesogens will switch back to initial state under strong depolarized field and shows transient memory (<1 min). But in nNiO/FLC composite sample, the impurity ions get trapped on the unsaturated surface sites of nNiO during their travel to opposite electrode on application of external bias. This reduces the screening of external bias field and offers a low voltage switching (~4 V). When the bias field is switched off, the nNiO/FLC composite tend to stay in the same state (memory) for long duration (~up to 20 min) owing to the reduced depolarization field. Thus, the adsorption of impurity ions in ZLI 3654 material by nNiO offers a technique to fabricate low power operating memory device based on nNiO/FLC composite.

Conclusion

In summary, a low voltage driven electro-optical memory device is fabricated by dispersing nNiO into FLC host material. The drop off in operating voltage and non-volatile memory behavior of nNiO/FLC composite sample cell is confirmed through various electro-optical measurements. This enhancement in electro-optical memory of nNiO/FLC composite device is attributed to the reduction in depolarization field by adsorption of impurity ions on to the surface of nNiO. Also, fast aligning of dipolar nNiO and mesogens in the nNiO/FLC composite, along the direction of applied electric field and reduced screening effect offered the low voltage operation of the composite. These studies elucidate the way for fabricating low power operating electro-optical memory devices for advanced information storage applications.

Acknowledgements

The authors sincerely thank the Director, CSIR – National Physical Laboratory, New Delhi for continuous encouragement and interest in this work. The author Achu Chandran is thankful to Council of Scientific and Industrial Research (CSIR) for providing financial assistance and the author Jai Prakash is grateful to the Department of Science and Technology (DST) for supporting this work under the INSPIRE Faculty Award (DST/INSPIRE Faculty Award/2011) through the INSPIRE Faculty Scheme of DST [IFA-PH-10]. Also, the author A. M. Biradar is thankful to DST (GAP-150632) and CSIR (Emeritus Scientist Scheme) for supporting this work.

References

1 R. J. Tseng, C. Tsai, L. Ma, J. Ouyang, C. S. Ozkan and Y. Yang, *Nat. Nanotechnol.*, 2006, **1**, 72–77.
2 I. A. Rousseau and P. T. Mather, *J. Am. Chem. Soc.*, 2003, **125**, 15300–15301.
3 B. S. Lee, B. C. Chun, Y. C. Chung, K. I. Sul and J. W. Cho, *Macromolecules*, 2001, **34**, 6431–6437.
4 Y. C. Chiu, C. L. Liu, W. Y. Lee, Y. Chen, T. Kakuchi and W. C. Chen, *NPG Asia Mater.*, 2013, **5**, e35.
5 M. Ebara, K. Uto, N. Idota, J. M. Hoffmana and T. Aoyagi, *Soft Matter*, 2013, **9**, 3074–3080.
6 L. Liu and P. Sharma, *Phys. Rev. E*, 2013, **88**, 040601(R).
7 Z. Hu, M. Tian, B. Nysten and A. M. Jonas, *Nat. Mater.*, 2009, **8**, 62–67.
8 W. Iglesias, N. L. Abbott, E. K. Mann and A. Jakli, *ACS Appl. Mater. Interfaces*, 2012, **4**, 6884–6890.
9 M. Tyagi, A. Chandran, T. Joshi, J. Prakash, V. V. Agrawal and A. M. Biradar, *Appl. Phys. Lett.*, 2014, **104**, 154104.
10 H. Ren, Y.-H. Fan and S.-T. Wu, *Appl. Phys. Lett.*, 2003, **83**, 1515–1517.
11 K. M. Johnson, D. J. McKnight and I. Underwood, *IEEE J. Quantum Electron.*, 1993, **29**, 699–714.
12 T. Araki, M. Buscaglia, T. Bellini and H. Tanaka, *Nat. Mater.*, 2011, **10**, 303–309.
13 F. Serra, M. Buscaglia and T. Bellini, *Mater. Today*, 2011, **14**, 488–494.
14 N. A. Clark and S. T. Lagerwall, *Appl. Phys. Lett.*, 1980, **36**, 899.
15 A. K. Thakur, S. Kaur, S. S. Bawa and A. M. Biradar, *Appl. Opt.*, 2004, **43**, 5614–5617.
16 H. Qi and T. Hegmann, *J. Mater. Chem.*, 2008, **18**, 3288–3294.
17 J. W. Goodby, R. Blinc, N. A. Clark, S. T. Lagerwall, M. A. Osipov, S. A. Pikin, T. Sakurai, K. Yoshino and B. Zeks, *Ferroelectric Liquid Crystals*, Gordon and Breach, Amsterdam, 1991, Part II, p. 410.
18 C. Blanc, D. Coursault and E. Lacazec, *Liq. Cryst. Rev.*, 2013, **1**(2), 83–109.
19 S. Kaur, S. P. Singh, A. M. Biradar, A. Choudhary and K. Sreenivas, *Appl. Phys. Lett.*, 2007, **91**, 023120.
20 A. Chandran, J. Prakash, P. Ganguly and A. M. Biradar, *RSC Adv.*, 2013, **3**, 17166–17173.
21 R. Basu, *Phys. Rev. E*, 2014, **89**, 022508.
22 M. Petrov, B. Katranchev, P. M. Rafailov, H. Naradikian, U. Dettlaff-Weglikowska and E. Keskinova, *J. Mol. Liq.*, 2013, **180**, 215–220.
23 A. Kumar and A. M. Biradar, *Phys. Rev. E*, 2011, **83**, 041708.

24 *Synthesis, Properties and Applications of Oxide Nanoparticles*, ed. J. A. Rodríguez and M. Fernández-García, Wiley, New Jersey, 2007.
25 M. Kreuzer, T. Tschudi, W. H. de Jeu and R. Eidenschink, *Appl. Phys. Lett.*, 1993, **62**, 1712.
26 A. Jakli, L. Almasy, S. Borbely and L. Rosta, *Eur. Phys. J. B*, 1999, **10**, 509–513.
27 W.-K. Lee, J.-H. Choi, H.-J. Na, J.-H. Lim, J.-M. Han, J.-Y. Hwang and D.-S. Seo, *Opt. Lett.*, 2009, **34**, 3653–3655.
28 T. Joshi, A. Kumar, J. Prakash and A. M. Biradar, *Appl. Phys. Lett.*, 2010, **96**, 253109.
29 E. Ruckenstein and H. Y. Hu, *Appl. Catal., A*, 1999, **183**, 85–92.
30 J. F. Bobo, L. Gabillet and M. Bibes, *J. Phys.: Condens. Matter*, 2004, **16**, S471–S496.
31 A. M. Soleimanpour, S. V. Khare and A. H. Jayatissa, *ACS Appl. Mater. Interfaces*, 2012, **4**, 4651–4657.
32 S. Vijayakumar, S. Nagamuthu and G. Muralidharan, *ACS Appl. Mater. Interfaces*, 2013, **5**, 2188–2196.
33 D. Adler and J. Feinleib, *Phys. Rev. B: Condens. Matter Mater. Phys.*, 1970, **2**, 3112–3134.
34 M. Rubinstein, R. H. Kodama and S. A. Makhlouf, *J. Magn. Magn. Mater.*, 2001, **234**, 289–293.
35 K. Oka, T. Yanagida, K. Nagashima, H. Tanaka and T. Kawai, *J. Am. Chem. Soc.*, 2009, **131**, 3434–3435.
36 H. M. Lee, H.-K. Chung, H.-G. Park, H.-C. Jeong, J.-H. Kim, T.-K. Park and D.-S. Seo, *J. Nanosci. Nanotechnol.*, 2015, **15**, 8139–8143.
37 A. M. Biradar, S. Wrobel and W. Haase, *Phys. Rev. A*, 1989, **39**, 2693–2702.
38 K. H. Yang, T. C. Chieu and S. Osofsky, *Appl. Phys. Lett.*, 1989, **55**, 125–127.
39 S. H. Perlmutter, D. Doroski and G. Moddel, *Appl. Phys. Lett.*, 1996, **69**, 1182–1184.
40 G. Barbero and G. Durand, *J. Appl. Phys.*, 1990, **67**, 2678.
41 A. Chandran, J. Prakash, T. Joshi and A. M. Biradar, *J. Mol. Liq.*, 2014, **198**, 280–285.
42 T. Joshi, J. Prakash, A. Kumar, J. Gangwar, A. K. Srivastava, S. Singh and A. M. Biradar, *J. Phys. D: Appl. Phys.*, 2011, **44**, 315404.
43 W.-T. Chen, P.-S. Chen and C.-Y. Chao, *Jpn. J. Appl. Phys.*, 2009, **48**, 015006.
44 H.-Y. Chen and W. Lee, *Appl. Phys. Lett.*, 2006, **88**, 222105.
45 P.-S. Chen, C.-C. Huang, Y.-W. Liu and C.-Y. Chao, *Appl. Phys. Lett.*, 2007, **90**, 211111.
46 B. Gokul, P. Matheswaran, K. M. Abhirami and R. Sathyamoorthy, *J. Non-Cryst. Solids*, 2013, **363**, 161–166.
47 J. Gangwar, K. K. Dey, S. K. Tripathi, M. Wan, R. R. Yadav, R. K. Singh and A. K. Srivastava, *Nanotechnology*, 2013, **24**, 415705.
48 L. Duan, L. Li, Z. Xu and W. Chen, *Environ. Sci.: Processes Impacts*, 2014, **16**, 1462–1468.
49 T. Mahmood, M. T. Saddique, A. Naeem, S. Mustafa, N. Zeb, K. H. Shah and M. Waseem, *Chem. Eng. J.*, 2011, **171**, 935–940.
50 M. R. Castell, P. L. Wincott, N. G. Condon, C. Muggelberg, G. Thornton, S. L. Dudarev, A. P. Sutton and G. A. D. Briggs, *Phys. Rev. B: Condens. Matter Mater. Phys.*, 1997, **55**, 7859–7863.
51 A. M. Ferrari, C. Pisani, F. Cinquini, L. Giordano and G. Pacchioni, *J. Chem. Phys.*, 2007, **127**, 174711.
52 R. P. Schwarzenbach, P. M. Gschwend and D. M. Imboden, *Environmental Organic Chemistry*, John Wiley & Sons, Inc., Hoboken, New Jersey, 2nd edn, 2003.
53 D. Cappus, M. HaBel, E. Neuhaus, M. Heber, F. Rohr and H.-J. Freund, *Surf. Sci.*, 1995, **337**, 268–277.
54 D. L. Kokkin, D. Dewberry and T. C. Steimle, *Chem. Phys. Lett.*, 2014, **609**, 1–5.
55 S. Acharya, S. Kundu, J. P. Hill, G. J. Richards and K. Ariga, *Adv. Mater.*, 2009, **21**, 989–993.